

NAMT

92-040

**Transient Heat Transfer Effect on
the Pseudoelastic Behavior of
Shape-Memory Wires**

**P.H. Leo
T.W. Shield
University of Minnesota**

**O.P. Bruno
Georgia Institute of Technology**

Research Report No. 92-NA-040

November 1992

Sponsors

**U.S. Army Research Office
Research Triangle Park
NC 27709**

**National Science Foundation
1800 G Street, N.W.
Washington, DC 20550**

University Libraries
Carnegie Mellon University
Pittsburgh, PA 15213-3890

**Transient Heat Transfer Effects on the
Pseudoelastic Behavior of Shape-Memory Wires**

by

P. H. Leo

T. W. Shield

Department of Aerospace Engineering and Mechanics
University of Minnesota
Minneapolis, MN 55455

and

O. P. Bruno

Department of Mathematics
Georgia Institute of Technology
Atlanta, GA 30332-0160

Abstract

Experimental results of a displacement-controlled elongation of a shape-memory wire of Nickel-Titanium are presented. It is observed that the hysteretic strain-stress curves depend strongly on the strain rates at which the wire is extended. A theoretical model is proposed to explain this phenomenon. This model couples the fully time-dependent heat transfer in the wire to its quasi-static mechanical behavior through the temperature dependence of the transformation stress of the alloy. It accounts *quantitatively* for experimentally observed changes in the pseudoelastic hysteresis. The model presented here is different from others proposed in the literature, as it does not make use of a kinetic relation and accounts for the observed changes in the pseudoelastic hysteresis without parameter fitting. The results show that a model consisting of a single moving austenite-martensite interface is sufficient to predict the response of the wire over several decades of strain rate.

1. Introduction

The behavior of shape-memory alloys and other ‘smart’ materials is governed by a diffusionless phase transformation between a high temperature, low strain austenite phase and a low temperature, high strain martensite phase. Both the shape-memory effect and the pseudoelastic behavior of shape-memory alloys arise from the interplay of temperature and stress in the free energy of the alloy. In the shape-memory effect, an alloy deformed in its martensitic phase recovers its initial shape when heated into the stable austenite regime. Pseudoelasticity occurs when an alloy that is austenite at zero stress is stressed in such a way that martensite becomes stable. The ensuing transformation results in a large straining of the material at an essentially constant stress.

The roles of temperature and stress in the mechanics of shape-memory alloys are further intertwined because heat is generated during a transformation from austenite to martensite. The heat generated as an austenite–martensite interface propagates alters the relative stability of the austenite and martensite phases at the interface, which, in turn, affects the growth of the interface. In this paper, we demonstrate the interaction between heat transfer and stress by conducting a series of experiments using Nickel–Titanium (NiTi) shape-memory wires. We then present a theoretical model that exhibits qualitative and quantitative agreement with the observed phenomena.

We experimentally study the pseudoelastic behavior of NiTi wires as a function of the imposed strain rate and the heat transfer between the wire and its surroundings. We observe that the pseudoelastic hysteresis increases as the imposed strain rate increases, and decreases as the heat transfer from the wire increases. Our models of these phenomena combine nonlinear thermoelastic models of diffusionless transformations with a heat flow problem that includes latent heat generation at a two phase interface. The thermoelasticity models are based on the assumption that the energy of the system is a function of both strain and temperature. At high temperatures, this energy has only one minimum, corresponding to the austenite phase, while at low temperatures there is a single minimum associated with martensite (or several minima representing the symmetry-related variants of martensite). At intermediate temperatures there may be mixtures of austenite and martensite, and there is a particular stress, the Maxwell stress, at which the two phases are in equilibrium. This Maxwell stress increases with temperature, so that if the temperature of the system increases, the stress needed to drive a transition from austenite to martensite also increases.

In our model, the austenite–martensite interface will not move unless the stress in the wire reaches a certain transition stress $\bar{\sigma}(\theta)$ associated with the temperature θ of the interface.

This transition stress is the sum of the thermodynamic Maxwell stress plus an additional stress σ_{hyst} equal to half the height of the isothermal hysteresis loop. The Maxwell stress arises from the free energy of the system, and so depends on the state of the system, while the additional stress accounts for dissipative processes associated with the phase change, which have been experimentally observed to be essentially independent of temperature (in isothermal experiments).

If we consider the case in which there is a single austenite-martensite interface in the wire, then higher strain rates require the interface to move faster. This results in an increase of the temperature of the interface as a result of the heat generated in the transformation from austenite to martensite. For the transformation to proceed, the stress in the wire must increase in order to match the transition stress at the elevated interface temperature. Even if we allow nucleation of new martensitic regions, we will still have a direct correlation between the overall heating of the wire and the stress required for the austenite to martensite region to grow. Finally, heat transfer between the wire and its surroundings also affects the temperature distribution along the wire, and therefore plays an important role in the phenomenon under consideration.

Experimental results of a similar nature to those presented here have been presented by Otsuku and Shimizu [1] and McCormick, et al. [2] in their study of NiTi alloys. Much of the previous modeling of shape-memory alloys has focused on isothermal transitions. Müller [3] and Müller and Xu [4] have described the temperature dependence of the pseudoelastic hysteresis loops in isothermal experiments, and linked the very existence of such loops to interfacial or coherency effects. They observed, like us, that the height ($= 2\sigma_{\text{hyst}}$) of isothermal hysteresis loops of the wire are essentially independent of temperature. Falk [5] has constructed a smooth polynomial energy function that captures, at least partially, the mechanics of the phenomena under consideration. In fact, the quasi-static mechanical description in our model is based on a modified version of Falk's model (or, alternatively, Knowles trilinear model [6]) that accounts for an additional stress σ_{hyst} .

The quasi-static motion of an austenite-martensite interface has also been studied by Abeyaratne and Knowles [7]. They postulate that there is a kinetic relation $V = V(\theta, \sigma)$ that gives the speed V of the interface as a function of the stress σ and the (uniform) temperature θ . Abeyaratne and Knowles derive an explicit expression for the function V based on an idealized model. However, the function V may be strongly dependent on σ , reflecting the fact that slow interface motions occur at nearly fixed stress. In contrast, our approach considers that the position of the interface is determined to insure that the overall behavior of the wire is quasi-static, thus we do not need to consider additional kinetic relations for the interface.

2. Experiments and Motivation

Nickel Titanium wires were tested in displacement control in an Instron 4502 screw driven mechanical testing machine. The wires were supplied by the Flexmedics Corp., Minneapolis, MN; their properties are listed in Table 1. The full load 20 kN load cell was used to provide as stiff a testing frame as possible. The wires were gripped in wedge grips with a length of 130 mm of wire between the grips. The displacement was measured as the overall displacement of the cross head; the difference between this measurement and the actual wire extension is negligible due to the stiffness of the load frame and the small loads and large deformations present in the wire. All load and displacement information, as well as readings from the five thermocouples discussed below, were recorded using a 386 class computer.

The temperature changes along the length of the wire were measured by attaching 5 thermocouples at 20 mm intervals to one specimen. The thermocouples were attached by covering the wire in 1/32 inch internal diameter Tygon tubing, making slits around half of the circumference of the tube at the locations for the thermocouples, and inserting the thermocouples through the slits. While this procedure results in poor contact between the wire and the thermocouple, it does not cause any mechanical changes to the wire, and it allows us to get a qualitative picture of the temperature response of the wire.

Figure 1 shows the stress-strain behavior of a NiTi wire at three strain rates. These strain rates correspond to extension rates of 0.5 mm/min, 5.0 mm/min and 50. mm/min; we will refer to the extension values in the following. Upon loading, we observe an initial elastic loading of the austenite phase, followed by a relatively constant stress plateau region associated with the austenite to martensite transition, and then another elastic loading stage, this time of the martensite phase. Unloading follows essentially the reverse path, but there is a pseudoelastic hysteresis between the austenite to martensite transition stress and the reverse martensite to austenite transition stress. Of particular interest here is the observation that the austenite to martensite transition stress increases with strain rate while the martensite to austenite stress decreases with strain rate, so the overall size of the hysteresis grows significantly as the strain rate increases.

The amount of this strain rate effect depends very strongly on the heat transfer characteristics between the wire and the surrounding medium. Figure 2 shows the stress-strain curves at the same strain rates when the wire is surrounded by a water bath. The increase in hysteresis with strain rate is greatly reduced by the increase in heat transfer between the wire and the water. We also see that the lowest rate experiments in both air and water are comparable, suggesting an approximately isothermal response.

We may also make two general observations about the behavior of the wire by looking at the different shapes of the stress-strain curves. First, we note that the loading and unloading paths of the martensite show different slopes, indicating that a secondary transformation may be occurring at higher stress levels. It is known [8] that the austenite to martensite transformation in NiTi occurs in two stages, with the austenite first transforming to an intermediate temperature martensite phase and then to a low temperature martensite phase. This phenomenon may also explain the upturn in high (50 mm/min) rate curve after roughly half the transformation is complete: the higher stress levels at this strain rate cause the second stage transformation to occur earlier in the loading history. Second, we notice that the stress-strain curve for the intermediate (5 mm/min) rate shows several sawtooth-like irregularities in the plateau portion of the curve. This behavior, which is highly repeatable, may be related to distinct nucleation events as discussed below.

Figures 3-5 show the temperature histories of the wire (prepared as described above) for the three different strain rates, as determined by five thermocouples placed at evenly spaced intervals along the wire. In the slowest strain rate case (Figure 3), we find that as the transformation front passes each thermocouple, it causes a temperature rise, which quickly decays as the front progresses. The data in Figure 3 shows that the transformation proceeds first from thermocouples 1, 2 and 3, and then encounters thermocouples 5 and 4. This indicates that a single transformation interface starts at the low end of the wire, followed by a second front nucleating at the other end. This order is repeatable, suggesting that the nucleation events are fixed by microscopic flaws and/or by the action of the grips.

Figure 4 shows the temperature profile for the intermediate (5 mm/min) rate. We find the same ordering as in the slow strain rate case, suggesting a similar progression of transformation fronts. However, in this case after the transition passes a given thermocouple, there is insufficient time for the heat to transfer out of the wire before the test is completed. This results in an overall rise in the wire temperature and hence the stress level. In contrast, the results at the highest rate shown in Figure 5, are quite different from the results in Figures 3 and 4. Here, there seems to be an overall heating along the length of the wire rather than the relatively uniform jumps from thermocouple to thermocouple indicative of individual interfaces. Thus, at this high strain rate there appear to be many active transformation fronts, which results in an even heating of the wire.

The ideas above are confirmed by optical observation of the wire during loading. By using a microscope objective attached to a video camera with suitable lighting, one can observe the passage of the interface, because the large strain involved in the transformation forms a slight kink on the wire surface. At elongation rates of both 0.5 mm/min and 5 mm/min a bright band is clearly visible moving along the wire. The timing of the appearance of

the bright band is very repeatable and occurs at the same point during the loading of the specimen each time. However, at a rate 50 mm/min this phenomena is not visible, which agrees with the conclusions reached above.

One final experiment was performed in order to determine the temperature dependence of the isothermal transition stress. For experimental purposes, this stress is taken as the plateau of the stress-strain curve in the low strain rate case. To find the temperature dependence of this stress we enclosed the wire in a temperature controlled water chamber positioned between the grips of the load frame. The transition stresses from three tests at 15 °C, 10 °C and 5 °C were used to determine the slope of the transition stress-temperature curve. A least squares fit of this data yields a slope of 7.6 MPa/°C.

3. Elasticity

The isothermal stress-strain behavior shown in Figures 1 and 2 can be described by using relatively simple one-dimensional models. For example, in the model developed by Falk [5], the Helmholtz free energy function F is taken to be a sixth order polynomial in the strain E ,

$$F(E, T) = \alpha E^6 - \beta E^4 + (\delta T - \gamma) E^2 + F_0(T), \quad (3.1)$$

where T is the absolute temperature, α , β , δ and γ are positive constants that depend on the material and $F_0(T)$ accounts for the heat capacity of the material. The free energy (3.1) is such that a zero strain austenite phase is stable at high temperatures, two martensite variants (at strains $\pm E_0$, where E_0 depends on α , β , γ and δ) are stable at low temperatures and a phase mixture is stable at intermediate temperatures.

The stress-strain behavior of a material that obeys Falk's model is shown in Figure 6. In this figure, we show the derivative of the free energy with respect to strain (thin solid line), which has both stable and unstable regimes, as well as the equilibrium stress-strain behavior (thick solid line). The equilibrium curve shows that the austenite deforms elastically until the stress increases to the Maxwell stress, which is the stress for which the shaded areas in the figure are equal. At this point, the austenite transforms to martensite at constant stress, so that the strain in the alloy increases as the volume fraction of martensite increases. Once the transformation is complete, any further deformation is accomplished by elastic deformation of the martensite. The unloading path is the reverse of the loading path; thus in the absence of thermodynamic barriers to prevent an equilibrium phase transition, there is no isothermal hysteresis in Falk's model and the Maxwell stress is identical to the austenite to martensite transition stress.

It is easy to show that (3.1) leads to a Maxwell stress that increases approximately linearly with temperature. For our purposes, it is convenient to include this feature of Falk's model in a simple, piecewise linear model. Therefore, we will use a simple variation of Falk's model in which the Maxwell stress depends linearly on temperature, the transformation strain ϵ^T and latent heat L are assumed to be independent of temperature, and both the austenite and martensite are taken to have a constant linear elastic modulus C' . This model is similar to the trilinear model used by Abeyaratne and Knowles [7] (the dashed lines in Figure 6), which approximates Falk's model by three straight line segments.

In Falk's model and the trilinear model, the equilibrium austenite to martensite and martensite to austenite transition stresses are identical to the Maxwell stress, so there is no isothermal hysteresis loop. This is clearly different from the experiments, and can be explained by noting that these simple models neglect any dissipative stresses that arise as the phases separate and new interface forms. The existence of such dissipative forces has been acknowledged in the work of Knowles and Abeyaratne [7] and Knowles [6], and Müller and Xu [4] have extended Falk's model to include such forces resulting from interfacial and/or coherency effects. Here, we allow for dissipative effects by taking the austenite to martensite transition stress to be equal to the Maxwell stress as determined above plus an additional constant stress σ_{hyst} equal to half the height of the isothermal hysteresis loop. That is, σ_{hyst} accounts for the isothermal hysteresis, which is assumed independent of temperature in the range of interest, while the temperature dependence of the Maxwell stress accounts for additional hysteresis owing to transient heat transfer.

4. One-dimensional heat transfer

Consider a shape-memory wire of length l_0 , and assume that the heat transfer properties of the austenite and martensite are identical. There are three mechanisms for the transfer of heat out of a segment of the wire: convection, radiation and conduction. The only source of heat in the wire is the latent heat L which is generated at an austenite martensite interface at position x_I and moving with speed v . If we imagine the wire to be cylindrical of radius r and we neglect temperature variations in r and take the surrounding medium to be isothermal, then a heat balance in an arbitrary control volume of the wire yields the partial differential equation,

$$\frac{\rho c_p}{k} \frac{\partial \theta}{\partial t} = \frac{\partial^2 \theta}{\partial x^2} - \frac{2h}{rk} (\theta - \theta_0) - \frac{2\sigma\epsilon_1}{rk} (\theta^4 - \theta_0^4) + \frac{L v}{k} \delta(x - x_I), \quad (4.1)$$

where $\theta(x, t)$ is the temperature in the wire, θ_0 is the temperature of the surrounding medium (which is also taken as the initial temperature of the wire) and δ is the Dirac delta function. In equation (4.1), the density of the wire is denoted by ρ , the thermal

conductivity by k , the convection coefficient by h and the heat capacity by c_p . Also, the radiation coefficient $\sigma = 5.669 \times 10^{-8} \text{ W/m}^2\text{K}^4$ and the emissivity of the surface is ϵ_1 .

The boundary conditions at $x = 0$ and $x = l_0$ depend on the detailed heat transfer at the grip-wire connection. In our models we have used both constant temperature ($\theta = \theta_0$ at $x = 0$ and $x = l_0$) and zero flux ($q = \frac{\partial \theta}{\partial x} = 0$ at $x = 0$ and $x = l_0$) boundary conditions. Based on our numerical results, and on the observation that the convective heat transfer term in (4.1) dominates over the conductive term, we conclude that insulated (no heat flux) boundary conditions are more appropriate. The implications of this choice will be discussed in more detail in the results section.

It is convenient to nondimensionalize equation (4.1) by introducing the thermal diffusivity $\alpha = k/\rho c_p$, then the nondimensional length is $x^* = x/l_0$ and the nondimensional time is

$$t^* = \frac{\alpha t}{l_0^2} . \quad (4.2)$$

By collecting nondimensional groups one finds

$$\frac{\partial \theta}{\partial t^*} = \frac{\partial^2 \theta}{\partial x^{*2}} - \beta^* (\theta - \theta_0) - \sigma^* \epsilon_1 (\theta^4 - \theta_0^4) + L^* v^* \delta(x^* - x_I^*), \quad (4.3)$$

where $\beta^* = 2l_0^2 h/\tau k$ is the convective Biot number, and so gives the relative importance of convection *vis* conduction, $\sigma^* = 2l_0^2 \sigma/\tau k$ plays a similar role in relating radiative and conductive heat transfer, and $L^* = L\alpha/k$ is the nondimensionalized latent heat.

Equation (4.3) can be solved using straightforward finite difference techniques. However, because of the latent heat source, Crank-Nicolson implicit methods perform badly [9]. Therefore we use a standard explicit method in discretizing equation (4.3), where we choose $\Delta t^*/(\Delta x^*)^2 = 0.1$ for all our calculations. An implicit method was also used to solve equation (4.3) in the absence of the nonlinear radiative term; no differences were found between the implicit and explicit solutions. The code was also checked against solutions for the moving boundary problem at constant interface speed [10]. These checks confirmed that our code worked well, except that the numerical solution showed a small peak in the temperature at the interface. We tried to smooth this peak by averaging the temperature over several nodal points behind the interface; this led to negligibly small changes in our results.

5. Coupling of Elasticity and Heat Transfer

Coupling between elasticity and heat flow occurs because the pseudoelastic phase transition involves a release of latent heat, which in turn affects the elasticity of the alloy. We now

analyze this coupling in the case in which there is a single interface associated with the transformation. Also, we only consider the loading (austenite to martensite) curve, though the reverse transformation can be treated in an analogous manner.

Consider stretching a shape-memory wire at some imposed rate of strain. Our main assumption is that for the austenite–martensite interface to propagate, the stress in the wire must be equal to the transition stress $\bar{\sigma}(\theta) = \sigma_M(\theta) + \sigma_{\text{hyst}}$ associated with the temperature θ of the interface. Because the strain of the wire will be accommodated by the formation of the high strain martensite phase (along with a smaller elastic stretch), the speed of the austenite–martensite interface will depend on the strain rate. Higher strain rates will lead to higher interfacial temperatures, so more stress must be applied to continue the phase transition. Because convection and radiation will act to moderate the interfacial temperature, increasing these effects will tend to keep the stress needed for the transformation nearer the isothermal value.

In order to examine how the interfacial speed couples the elasticity and heat transfer problems, consider the trilinear model discussed earlier. Suppose that at time t_0 the wire has a deformed length $l(t_0)$ and is under stress $\sigma(t_0)$. Also, the austenite–martensite interface is at the position $x_I(t_0)$ (as measured in the undeformed state of the wire) and is at the temperature $\theta(x_I(t_0), t_0)$. In the next time step Δt , the bar must increase in length by $\Delta l = \dot{\epsilon} l_0 \Delta t$, where $\dot{\epsilon}$ is the imposed strain rate. This additional length can be accommodated either elastically, by transforming austenite to martensite or by a combination thereof.

In order to decide what the position of the interface at time $t_0 + \Delta t$ will be, we find the transition stress $\bar{\sigma}(\theta(x_I(t_0), t_0))$ associated with the temperature $\theta(x_I(t_0), t_0)$ by using the trilinear model to find the Maxwell stress at $\theta(x_I(t_0), t_0)$ and adding the constant σ_{hyst} . We then calculate

$$\Delta l_1 = \frac{\bar{\sigma}(\theta(x_I(t_0), t_0)) - \sigma(t_0)}{C}, \quad (5.1)$$

where C is the modulus of the wire. The quantity Δl_1 is the total stretch that can be accommodated elastically when the stress in the wire is at $\bar{\sigma}(\theta(x_I(t_0), t_0))$. If $\Delta l \leq \Delta l_1$, the additional stretch of the wire will be achieved purely by elastic deformation, the new stress will be $\sigma(t_0 + \Delta t) = \sigma(t_0) + C\Delta l/l_0$, and the interface will not move, i.e., $x_I(t_0 + \Delta t) = x_I(t_0)$. Otherwise, $\Delta l > \Delta l_1$, and the bar will be stretched elastically up to the current transition stress $\bar{\sigma}$, and then, new martensite must form in order to accommodate the remaining deformation, so that

$$x_I(t_0 + \Delta t) = x_I(t_0) + \frac{\Delta l - \Delta l_1}{\epsilon_T}, \quad (5.2)$$

where ϵ^T is the transformation strain from austenite to martensite. In either case, the new position and speed $v = (x_I(t_0 + \Delta t) - x_I(t_0))/\Delta t$ of the interface are used by the heat transfer code to recalculate the temperature profile of the bar, and in particular the temperature at the new interface position, and the process is repeated until the entire bar has transformed to martensite.

We reiterate that we are only considering the loading curve of the shape-memory wire, though unloading can be modeled in much the same way by determining to what extent the interface cools upon transforming from martensite to austenite. Also, we are only calculating the additional hysteresis from the generation of heat at the interface; the isothermal hysteresis arises solely from the constant σ_{hyst} .

The discussion above focussed on the case where we assume that a single interface starts from one end of the wire and propagates to the other end. The transformation is completed when the interface reaches the end of the wire. Based on the experimentally obtained temperature profiles, we have considered two additional cases. In one, two interfaces propagate symmetrically from the ends of the wire toward the center. However, if the ends of the wire are assumed to be insulated, then the single interface model strain-stress curves do not differ significantly from those of the symmetric two interface model. In the second case, we have allowed for the possibility that nucleation may occur, so that the position of the actively transforming interface may change each time step. The results from this model will be discussed below.

6. Parameters

The comparison of our model results with experimental observations depends on knowledge of both the heat transfer and elasticity parameters for the NiTi wire used in the experiment. This data has proven difficult to obtain, as there is a lack of data on the thermal constants for NiTi and the elastic constants (and possibly the thermal constants) are extremely sensitive to the composition of the particular alloy. The values we have used for the various constants needed in our model have been taken from the recent literature and the value of the additional stress σ_{hyst} as well as the slope of the transition stress-temperature curve were obtained by the experiments described above.

The heat transfer constants needed for our model are the thermal conductivity k , the thermal diffusivity, α , the convection coefficient, h and the latent heat, L . The necessary elasticity parameters assuming the trilinear model are the elastic moduli, C , of the austenite and martensite phases (which are taken to be identical) and the transformation strain, ϵ^T . The values used, and their sources, are summarized in Table 1.

The two key parameters that describe the coupling between the thermal and mechanical problems are the latent heat, L and the slope η of the Maxwell stress versus temperature curve. The constant η for our material was determined experimentally as described above. However, the latent heat posed more of a problem, primarily because of the different transitions that are reported in the literature [8,11] and which we observed in calorimetry measurements. Thus we have taken the latent heat to be 43 J/cm^3 as given for the intermediate to high temperature transition for nickel rich NiTi in [8].

7. Results and Discussion

The experimental data at all strain rates is best matched by our single interface model with insulated ends. The numerical results for this case are shown in Figure 7 for convection in air and in Figure 8 for convection in water. In almost all cases we find excellent agreement with the initial linear rise of the stress-strain curve and the transition to the pseudoelastic plateau of the stress strain curve.

The details of the heat transfer in the wire provide insight in to the stress-strain response of the NiTi. Because we take the ends of the wire to be insulated, any initial motion of the transformation front (which is assumed to begin at one end of the wire) is accompanied by a large increase in temperature, and so the Maxwell stress must increase accordingly. However, a steady state among conduction, convection, radiation and the heat production is eventually reached where the temperature of the transformation front, and hence the transition stress, stays fairly constant. This corresponds to the plateau region of the stress strain curve. In fact, our model predicts that in air, this steady state temperature rise is about $2 \text{ }^\circ\text{C}$ for the slow rate (0.5 mm/min), $9 \text{ }^\circ\text{C}$ for the intermediate rate (5 mm/min) and $13 \text{ }^\circ\text{C}$ for the fast rate (50 mm/min), in agreement with experiments [2]. Finally, as the interface reaches the other end of the wire, the temperature begins to rise again because of the no flux boundary condition, and we observe a slight increase in the stress strain behavior as the wire completes its transformation to martensite. We note that had we chosen constant temperature boundary conditions at the ends of the wire, the initial stress rise would be less steep, and a downturn in the stress would appear as the transformation nears completion.

One of the most pronounced differences between our model results and the experimental data is in the behavior of the wire under the fast (50 mm/min) loading rate in air. In this case, the model correctly finds the transformation plateau, but experiments show that about half way through the transformation, the plateau region acquires a pronounced positive slope that is not reproduced by the model. We speculate that because of the high stresses in the high rate case, the low temperature martensite phase in NiTi may begin to

form at this point. Because the austenite to low temperature martensite has a latent heat about three times greater than the austenite to intermediate phase transition, one would expect a significant generation of heat associated with the low temperature phase, which could account for the marked increase in the transformation stress. This behavior is not observed at any of the lower strain rates; however, the fact that in all cases the loading and unloading slopes of the martensitic phase are different may also indicate the possibility of a secondary martensitic transformation.

Another difference between theory and experiment occurs when we consider the fast loading of the wire in water. We expect in this case that a local increase in the temperature of the hollow tube of water surrounding the wire accounts for significant heat transfer from the wire. The upper numerical curve in figure 8 includes a correction to the specific heat of the wire to include the specific heat of the surrounding water. In the future a two dimensional heat transfer model could be used to eliminate this discrepancy.

The fact that we have assumed a single interface exists arises both from our experimental observations and the idea that nucleation in first-order phase transformations involves overcoming some energy barrier. In order to better understand this latter point, we have considered models where more than one interface is allowed to nucleate in the wire. Consider first the case where at each time step, a new interface is formed at the coldest point of the wire (i.e, there is no energy barrier). Because the initial interface does not move far enough to generate a significant temperature rise, there is no initial rise in the transformation stress. Instead, the temperature increase in the wire depends on the volume fraction of transformed martensite through essentially a bulk heating, and so the model predicts a linear increase in transformation stress as the transformation proceeds, which is clearly different from the experimental data. These results for the intermediate strain rate case are shown by the dashed curve in Figure 9.

We obtain better results when we allow for an energy barrier and assume nucleation occurs only if the temperature of the active interface is greater than some assigned threshold value above the temperature of the coldest part of the wire. Figure 9 shows such a case for a threshold of 16. °C for an elongation rate of 5 mm/min. Here, we observe the initial rise from the isothermal transition stress to the dynamic transition stress, because no nucleation occurs during this stage. During the transformation, however, there are a discrete number of nucleation events to a new active transformation front. These events are accompanied by a sharp drop in stress, owing to the fact that this new front is at a much lower temperature. This behavior appears qualitatively similar to the 'kinks' in the experimental stress-strain curves at the intermediate strain rate, suggesting that these kinks may correspond to discrete nucleation events. Unfortunately, our multiple nucleation

model does not work as well when the elongation rate is fast (50 mm/min), which is the case where multiple nucleation events are observed to occur. This may be due to the fact that there are multiple active fronts in the high rate case (as suggested by the uniform heating observed), while our model is limited to a single active interface at any one time.

8. Summary and Conclusions

In this paper, we have shown that both the transition stress and the size of the pseudoelastic hysteresis in NiTi shape-memory wires depends on the strain rate of the experiment. These effects can be modeled by coupling the temperature and stress dependence of the free energy of the alloy with the heat transfer problem associated with the moving austenite-martensite interface. That is, the behavior of the wire, at least in deformation controlled experiments, can be explained by assuming quasi-static elastic behavior together with transient heat transfer.

The main conclusions that we draw are the following:

At low strain rates, a single interface moving through the wire appears to dominate the transformation. This interface moves slowly enough so that the heat generated at the interface is quickly dissipated, and thus this case approximates isothermal behavior.

At intermediate strain rates, a single interface again seems to dominate the transformation. This interface moves fast enough so that the heat generated by the transformation causes a significant increase in the amount of hysteresis. While there is some evidence to suggest that the active austenite-martensite front may jump from position to position at discrete times, this does not affect the overall behavior of the wire.

At high strain rates, experiments indicate that there are multiple active transformation fronts during the transformation. However, the model that best matches the experiment is again the single interface model. In this case, we also notice a significant rise in the transformation stress about halfway through the transformation, suggesting that different phenomena, such as a secondary transformation, may be occurring. Thus, we expect that accurate models at much higher strain rates than those considered here would have to take into account both changes in the atomic mechanisms of the transformation as well as dynamic elasticity effects.

The time scales in all the experiments indicate that convection is the dominant heat transfer mode. Thus, the best agreement between theory and experiment occurs when the grips are modeled as insulated.

9. Acknowledgment

PHL would like to acknowledge the support of the Army Research Office (grant No. DA/DAAL03-89-G-0081), the Alcoa Foundation and the Center for Nonlinear Analysis at Carnegie Mellon University. TWS would like to acknowledge the National Science Foundation (thru the NYI program), the Office of Naval Research (grant No. N/N00014-91-J-4034) and the McKnight Foundation for their support. OPB would like to acknowledge the support of the National Science Foundation (grant No. DMS-9200002).

We would also like to thank R. D. James, R. Abeyaratne and J. K. Knowles for many helpful discussions and the Flexmedics Co. of Minneapolis, MN for providing the NiTi wire specimens.

9. References

1. Otsuku, K. and Shimizu, K., "Pseudoelasticity and Shape Memory Effects in Alloys," *Int. Metals Review*, **31**, pp. 93-114, 1986.
2. McCormick, P. G., Miyazaki, S. and Liu, Y., "Intrinsic Transformation Influenced Mechanical Behaviour in a NiTi Alloy," proceedings of International Conference on Martensitic Transformation (ICOMAT-92), in press.
3. Müller, I., "On the Size of the Hysteresis in Pseudoelasticity," *Cont. Mech. Thermod.*, **1**, pp. 125-142, 1989.
4. Müller, I., and Xu, H., "On the Pseudo-Elastic Hysteresis," *Acta metall.*, **39** (3), pp. 263-271, 1991.
5. Falk, F., "Model Free Energy, Mechanics, and Thermodynamics of Shape Memory Alloys," *Acta Metall.*, **28**, pp. 1773-1780, 1980.
6. Knowles, J. K., "On the Dissipation Associated with Equilibrium Shocks in Finite Elasticity," *J. Elasticity*, **9**, pp. 131-158, 1979.
7. Abeyaratne, R., and Knowles, J. K., "A Continuum Model of a Thermoelastic Solid Capable of Undergoing Phase Transitions," Tech. rpt. no. 7, Cal. Tech., 1992.
8. *Shape Memory Alloys*, H. Funakubo ed., J. B. Kennedy translator, Gordon and Breach Science Publishers, New York, 1986.
9. Smith, G. D., *Numerical Solution of Partial Differential Equations: Finite Difference Methods*, Clarendon Press, Oxford, 1978.

10. Sekerka, R. F., Jeanfils, C. L. and Heckel, R. W., "The Moving Boundary Problem," in *Lectures on the Theory of Phase Transformations*, H. I. Aaronson, ed., TMS-AIME, New York, 1975.
11. Miyazaki, S., Kimura, S. and Otsuka, K., "Shape-memory Effect and Pseudoelasticity Associated with the R-Phase Transition in Ti-50.5 at% Ni Single Crystals," *Philosophical Magazine*, **57** (3), pp. 467-478, 1988.
12. Holman, J. P., *Heat Transfer*, McGraw-Hill, New York, 1986.
13. Hodgson, D. E., Wu, M. H., and Biermann, R. J., "Shape-Memory Alloys," in *Metals Handbook*, 10th edition, Vol. 2., ASM International, Materials Park Ohio, pp. 897-902, 1990.
14. Smith, J. F., Jiang, R. L., and Predel, B., " C_p and Fractal Phase Transformation in Shape Memory Alloy Ni-52Ti," *Materials Science and Engineering*, **A149**, pp. 111-120, 1991.

Table 1. The properties of the Nickel-Titanium wires used in the experiments.

Property	Value	Symbol, Source
Composition	50.5 Ni (at %)	
Area	0.3339 mm ²	[*]
Length	130. mm	l_0 , [*]
Thermal diffusivity	0.06 cm ² /s	α , [14]
Conduction	0.2 J/cm-s-°K	k , [13]
Convection (air)	6.5×10^{-4} W/cm ² -°K	h , [12]
Convection (water)	8.90×10^{-2} W/cm ² -°K	h , [12]
Specific heat (300 °K)	0.5 J/gm-°K	c_p , [14]
Latent heat	43. J/cm ³	L , [8]
Density	6.45 g/cm ³	ρ , [13]
Elastic modulus	30 GPa	C , [*]
Emissivity	1.0	ϵ_1
Transition stress (300 °K)	360 MPa	σ^T , [*]
Transition strain	.068	ϵ^T , [*]
Slope of $\bar{\sigma}(\theta)$	7.6 MPa/°K	η , [*]
Width of hysteresis loop		$2\sigma_{\text{hyst}}$, [*]

[*] indicates measured quantities.

Figure Captions

Figure 1. The stress-strain response of a NiTi wire in tension at strain rates of $6.4 \times 10^{-5} \text{ sec}^{-1}$ (0.5 mm/min) (solid curve), $6.4 \times 10^{-4} \text{ sec}^{-1}$ (5.0 mm/min) (thick curve) and $6.4 \times 10^{-3} \text{ sec}^{-1}$ (50.0 mm/min) (dashed curve) in air at 23 °C.

Figure 2. The stress-strain response of a NiTi wire in tension at strain rates of $6.4 \times 10^{-5} \text{ sec}^{-1}$ (0.5 mm/min) (solid curve), $6.4 \times 10^{-4} \text{ sec}^{-1}$ (5.0 mm/min) (thick curve) and $6.4 \times 10^{-3} \text{ sec}^{-1}$ (50.0 mm/min) (dashed curve) in water at 23 °C.

Figure 3. The temperature rises at the five thermocouples for an strain rate of $6.4 \times 10^{-5} \text{ sec}^{-1}$ (0.5 mm/min). The symbols denote the order of the thermocouples along the wire: 1. open square, 2. circle, 3. triangle, 4. inverted triangle and 5. solid square.

Figure 4. The temperature rises at the five thermocouples for an strain rate of $6.4 \times 10^{-4} \text{ sec}^{-1}$ (5.0 mm/min). The symbols denote the order of the thermocouples along the wire: 1. open square, 2. circle, 3. triangle, 4. inverted triangle and 5. solid square.

Figure 5. The temperature rises at the five thermocouples for an strain rate of $6.4 \times 10^{-3} \text{ sec}^{-1}$ (50. mm/min). The symbols denote the order of the thermocouples along the wire: 1. open square, 2. circle, 3. triangle, 4. inverted triangle and 5. solid square.

Figure 6. Schematic stress-strain behavior for a material having a free energy (3.1). The dark line shows the stress-strain behavior; the Maxwell stress σ_M is taken so that the two shaded areas are equal. The dashed line shows the trilinear approximation.

Figure 7. Predicted stress-strain results (thin curves) for a NiTi wire in air compared to the experimental data from figure 1 (thick curves). These results are for the case of a single moving interface and insulated ends of the wire. All relevant parameters are given in Table 1.

Figure 8. Predicted stress-strain results (thin curves) for a NiTi wire in water compared to the experimental data from figure 2 (thick curves). These results are for the case of a single moving interface and insulated ends of the wire. All relevant parameters are given in Table 1.

Figure 9. Predicted stress-strain results for a NiTi wire in air at a strain rate of $6.4 \times 10^{-4} \text{ sec}^{-1}$ (5.0 mm/min). These results are for the case of a multiple interfaces with a nucleation threshold of 16. °C (solid curve) and zero threshold (dashed curve) compared to the experimental data (thick curve). All relevant parameters are given in Table 1.

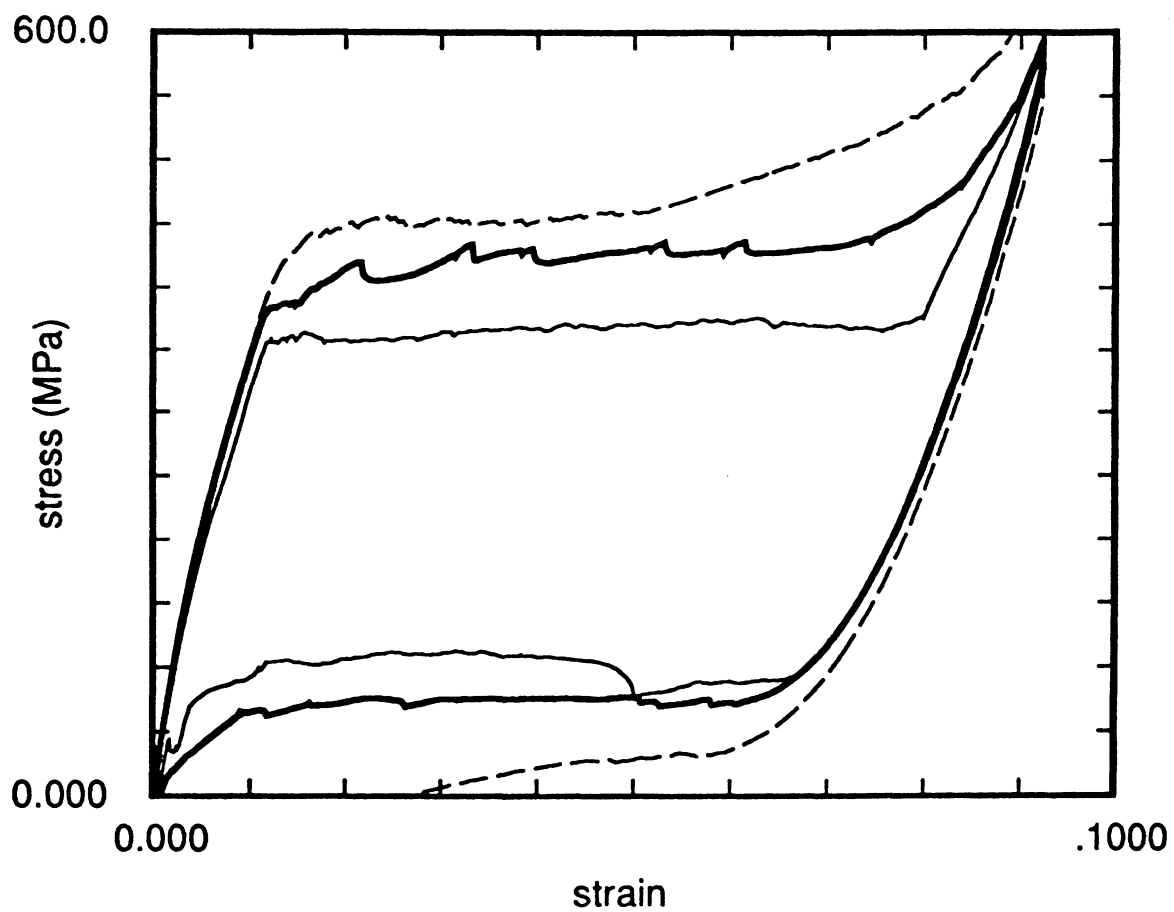


Figure 1. The stress-strain response of a NiTi wire in tension at strain rates of $6.4 \times 10^{-5} \text{ sec}^{-1}$ (0.5 mm/min) (solid curve), $6.4 \times 10^{-4} \text{ sec}^{-1}$ (5.0 mm/min) (thick curve) and $6.4 \times 10^{-3} \text{ sec}^{-1}$ (50.0 mm/min) (dashed curve) in air at 23 °C.

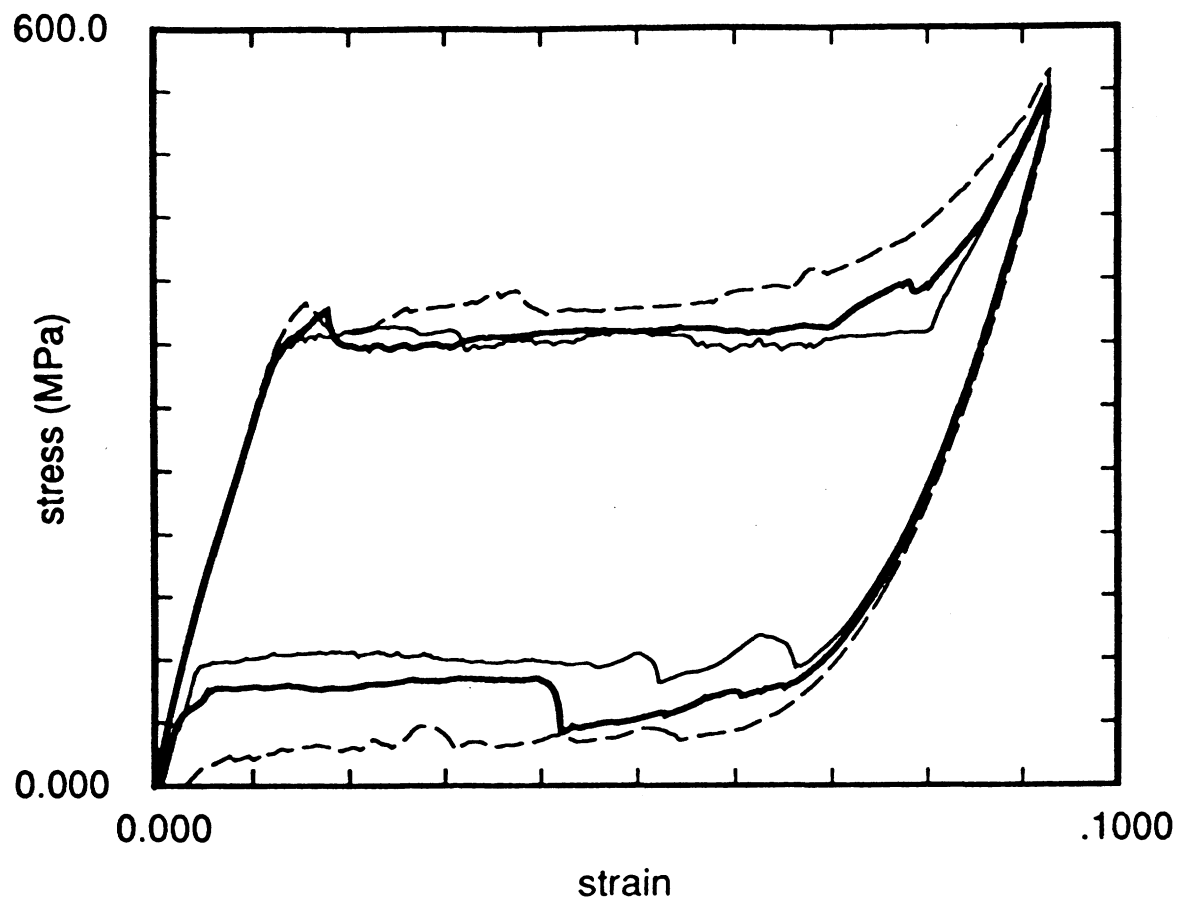


Figure 2. The stress-strain response of a NiTi wire in tension at strain rates of $6.4 \times 10^{-5} \text{ sec}^{-1}$ (0.5 mm/min) (solid curve), $6.4 \times 10^{-4} \text{ sec}^{-1}$ (5.0 mm/min) (thick curve) and $6.4 \times 10^{-3} \text{ sec}^{-1}$ (50.0 mm/min) (dashed curve) in water at 23 °C.

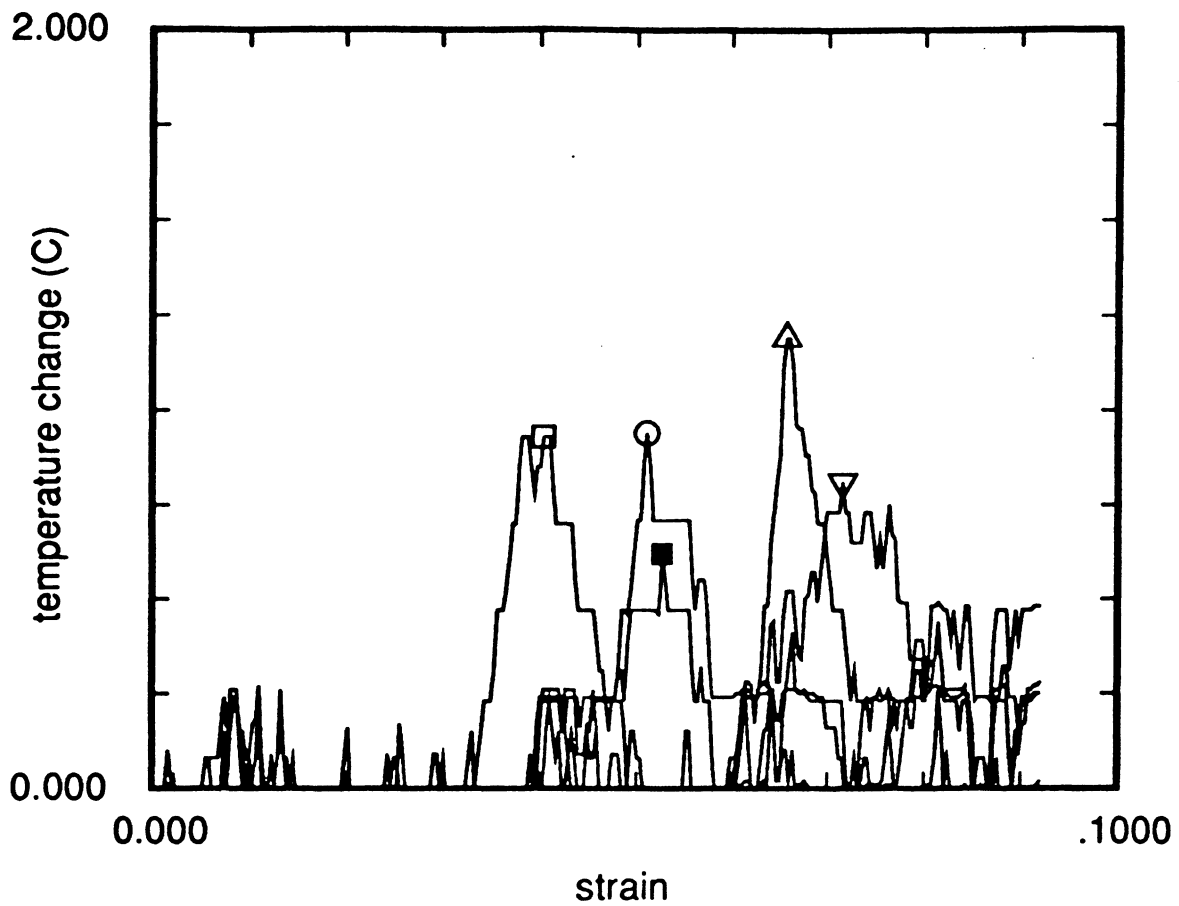


Figure 3. The temperature rises at the five thermocouples for an strain rate of $6.4 \times 10^{-5} \text{ sec}^{-1}$ (0.5 mm/min). The symbols denote the order of the thermocouples along the wire: 1. open square, 2. circle, 3. triangle, 4. inverted triangle and 5. solid square.

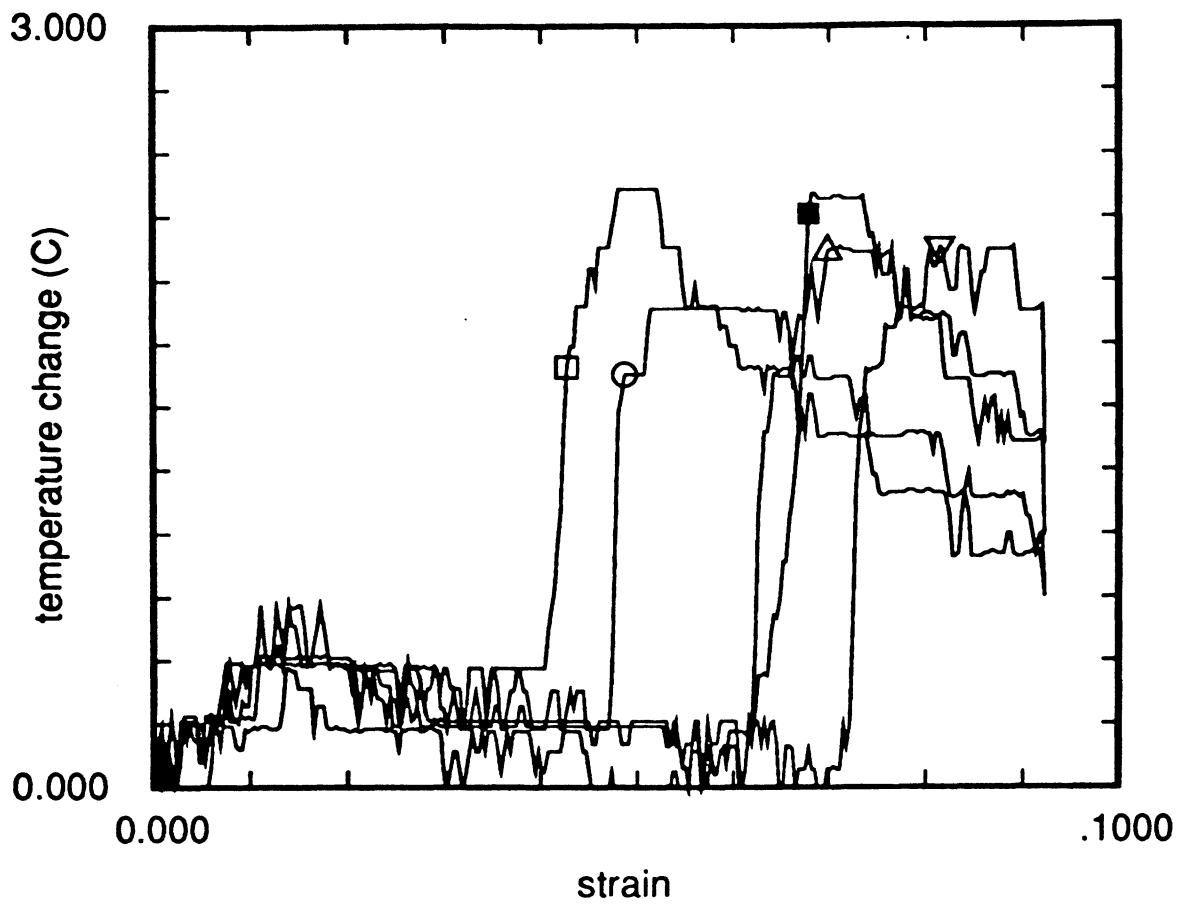


Figure 4. The temperature rises at the five thermocouples for an strain rate of $6.4 \times 10^{-4} \text{ sec}^{-1}$ (5.0 mm/min). The symbols denote the order of the thermocouples along the wire: 1. open square, 2. circle, 3. triangle, 4. inverted triangle and 5. solid square.

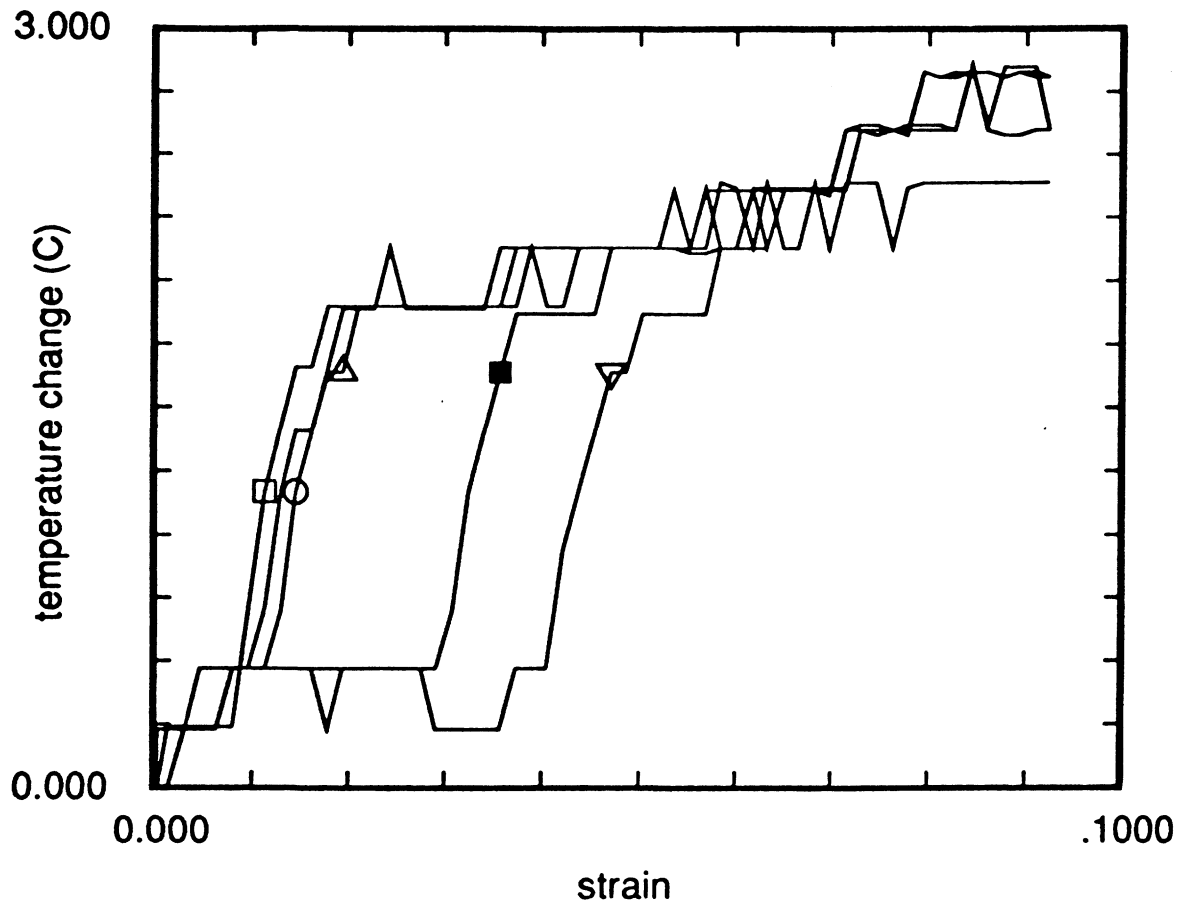


Figure 5. The temperature rises at the five thermocouples for an strain rate of $6.4 \times 10^{-3} \text{ sec}^{-1}$ (50. mm/min). The symbols denote the order of the thermocouples along the wire: 1. open square, 2. circle, 3. triangle, 4. inverted triangle and 5. solid square.

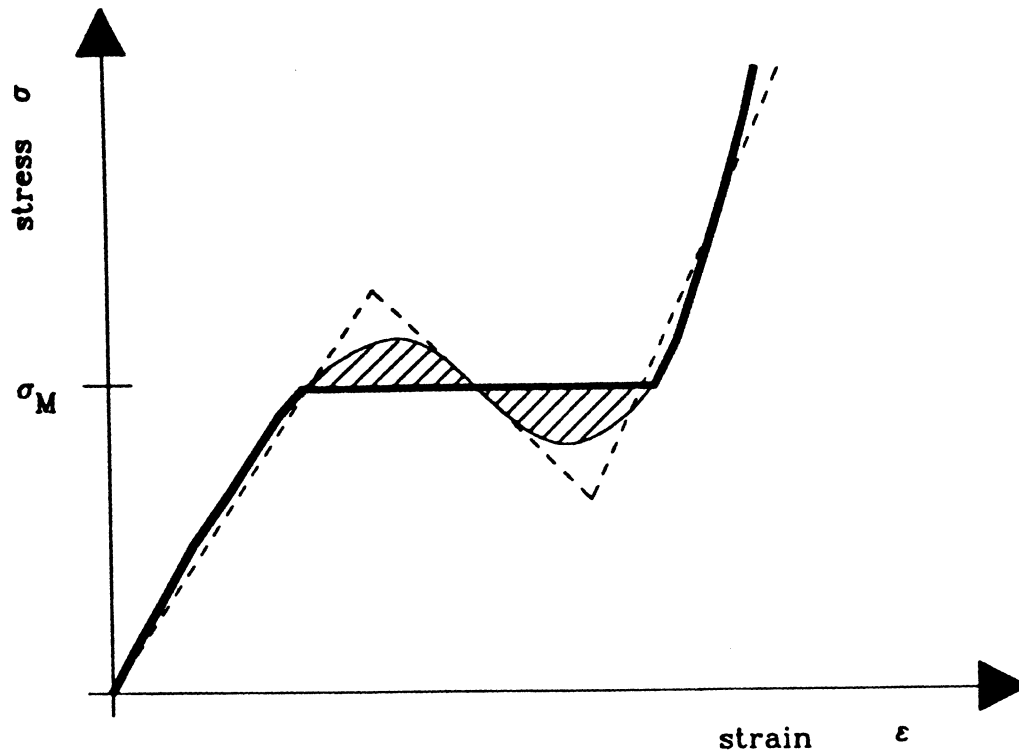


Figure 6. Schematic stress-strain behavior for a material having a free energy (3.1). The dark line shows the stress-strain behavior; the Maxwell stress σ_M is taken so that the two shaded areas are equal. The dashed line shows the trilinear approximation.

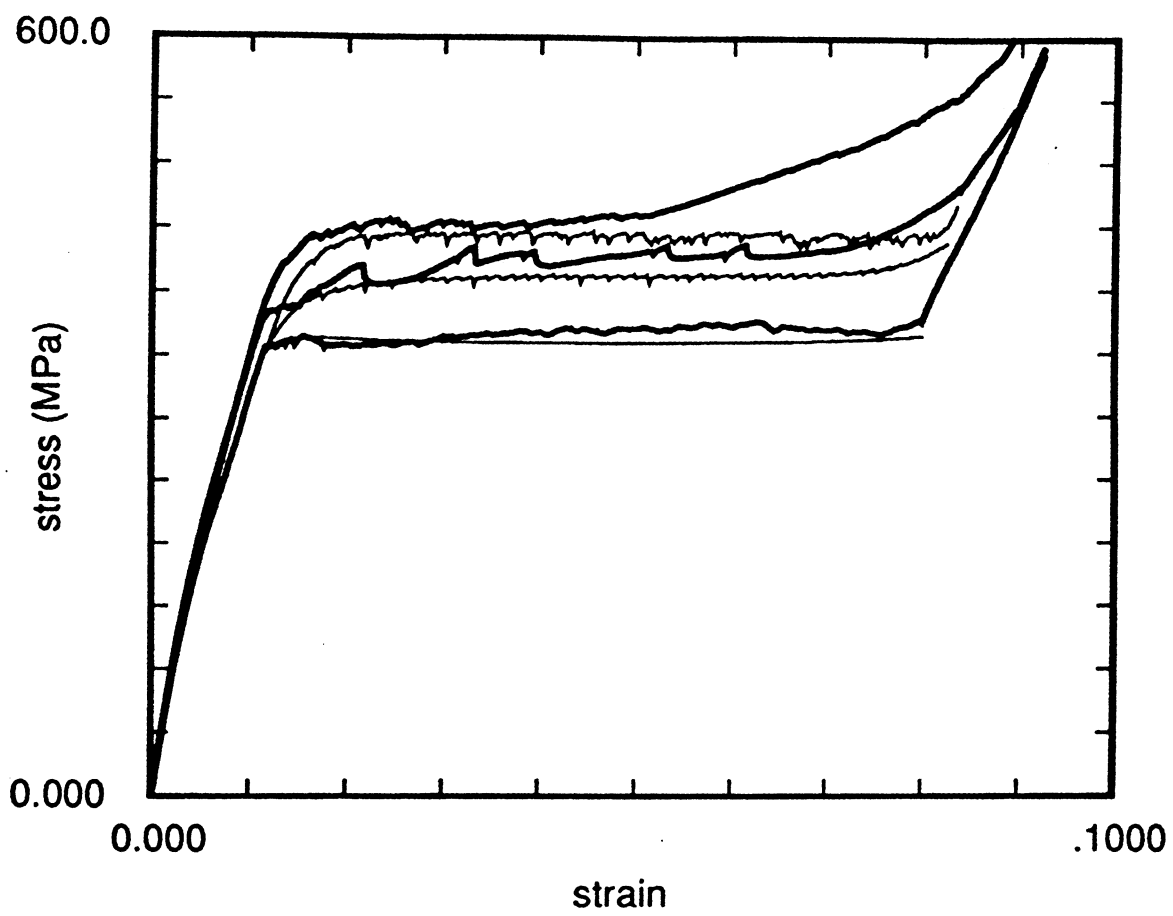


Figure 7. Predicted stress-strain results (thin curves) for a NiTi wire in air compared to the experimental data from figure 1 (thick curves). These results are for the case of a single moving interface and insulated ends of the wire. All relevant parameters are given in Table 1.

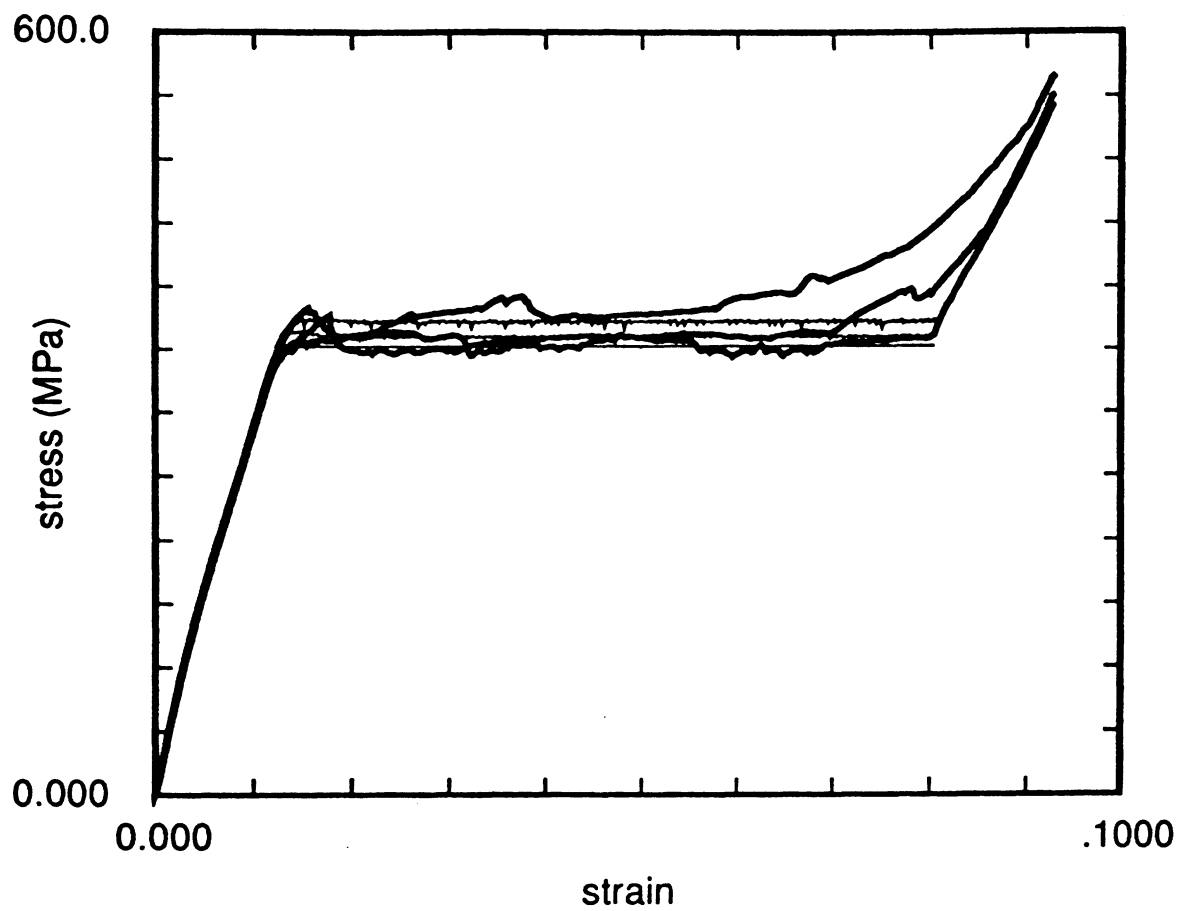


Figure 8. Predicted stress-strain results (thin curves) for a NiTi wire in water compared to the experimental data from figure 2 (thick curves). These results are for the case of a single moving interface and insulated ends of the wire. All relevant parameters are given in Table 1.

DEC 12 2003

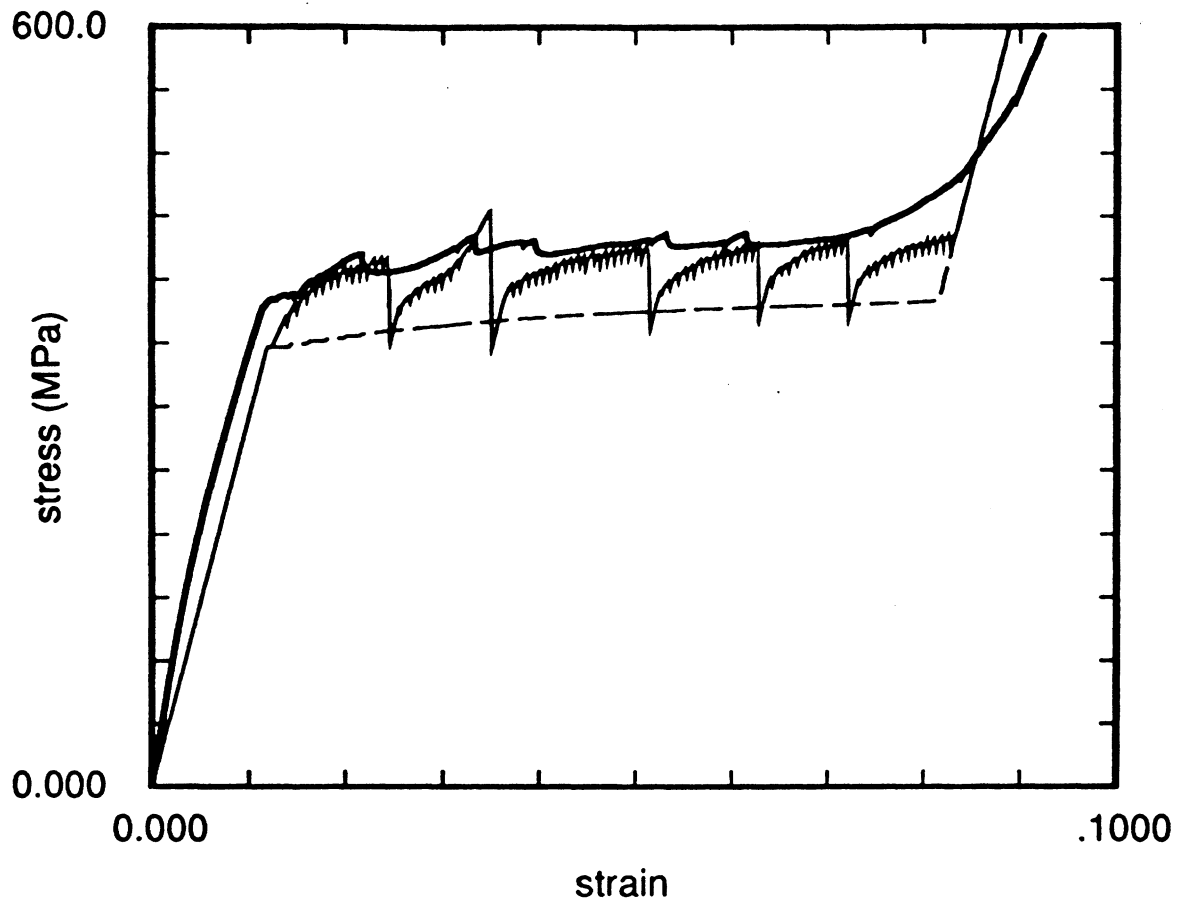


Figure 9. Predicted stress-strain results for a NiTi wire in air at a strain rate of $6.4 \times 10^{-4} \text{ sec}^{-1}$ (5.0 mm/min). These results are for the case of a multiple interfaces with a nucleation threshold of 16. °C (solid curve) and zero threshold (dashed curve) compared to the experimental data (thick curve). All relevant parameters are given in Table 1.